J. Fluid Mech. (2010), *vol.* 643, *pp.* 449–470.
doi:10.1017/S0022112009992230

Far-field disturbance flow induced by a small non-neutrally buoyant sphere in a linear shear flow

EVGENY S. ASMOLOV[1,2]† AND FRANÇOIS FEUILLEBOIS[3]

[1]Central Aero-Hydrodynamics Institute, 1 Zhukovsky str., Zhukovsky, Moscow region, 140180, Russia

[2]Institute of Mechanics, Lomonosov Moscow State University, 1 Michurinsky prosp., Moscow, 119192, Russia

[3]Laboratoire de Physique et Mécanique des Milieux Hétérogènes (PMMH), ESPCI, 10 rue Vauquelin, 75231 Paris cedex 05, France

(Received 26 January 2009; revised 11 September 2009; accepted 14 September 2009)

The disturbance flow due to the motion of a small sphere parallel to the streamlines of an unbounded linear shear flow is evaluated at small Reynolds number using the method of matched expansions. Decaying laws are obtained for all velocity components in a far inviscid region and viscous wakes. The z component (in the direction of the shear-rate gradient) of the disturbance velocity is cylindrically symmetric in the inviscid region. It decays with the distance r from the sphere like $r^{-5/3}$, while the y component (in the direction of vorticity) decays like $r^{-4/3}$. The widths of two viscous wakes, located upstream and downstream of the sphere, grow with the longitudinal coordinate x as $y_w \sim z_w \sim |x|^{1/3}$. The maximum x and z components of the velocity are located in the wake cores; they scale like $|x|^{-2/3}$ and $|x|^{-1}$ respectively. For two particles interacting through their outer regions, the migration velocity of each particle is the sum of the velocity of an isolated particle and of a disturbance velocity induced by the other one. Particles placed in the normal or transversal directions repel each other. When each particle is located in a wake of the other one, they may either attract or repel each other.

Key words: fluid inertia, low Reynolds number, shear flow, wake

1. Introduction

The disturbance flow induced by a non-neutrally buoyant sphere at small Reynolds number is governed, to leading order, by creeping-flow equations. Inertial terms are small compared with viscous ones at distances from the particle centre of the order of the particle radius, a (inner region). However, they decay with distance slower than the viscous terms and become of the same order at sufficiently large distances from the sphere (outer region). For a uniform undisturbed flow, the length scale of the outer region is the Oseen length $L_O = \nu/V_s$, where V_s is the magnitude of the particle slip velocity. The Oseen solution to the outer region describes also an inviscid flow and a viscous wake at large distances compared with L_O.

For a linear shear undisturbed velocity, studies of the disturbance flow in the outer region have been aimed at calculating the lift force on the particle due to small fluid inertia. For that purpose, Saffman (1965) introduced another length scale of the outer

† Email address for correspondence: aes@an.aerocentr.msk.su

region, $L_S = (\nu/G)^{1/2}$, based on the shear rate G, where the viscous and inertial terms balance. He showed that the particle effect in a far region is equivalent to a point force located at the centre of the sphere. The matching condition with the Stokeslet solution in the inner region may be satisfied if the point force is introduced into the momentum equation. The Stokeslet decays with the distance from the sphere like r^{-1}. As a result the disturbance velocity induced by a non-neutrally buoyant particle in the outer region is

$$u_{nnb} \sim V_s a/L_S. \tag{1.1}$$

No analytical solution similar to Oseen solution can be obtained for the linear shear flow. Oseen-like equations were solved in terms of the three-dimensional Fourier transform of the disturbance field. The flow induced by the sphere in the outer region looks in the inner region like a small uniform flow. For this reason, earlier works concentrated on this disturbance flow. Saffman (1965, 1968) calculated therefrom the migration velocity of a particle moving parallel to the streamlines of an unbounded flow for the strong shear limit when two small Reynolds numbers are related as $R_s = aV_s/\nu \ll R_G^{1/2} = a\,(G/\nu)^{1/2}$. The inequality means that the linear shear flow dominates over the uniform flow in the outer region. Harper & Chang (1968) and Miyazaki, Bedeaux & Avalos (1995) found the other components of the migration velocity when the sphere moves in an arbitrary direction relative to the shear flow. Asmolov (1990) and McLaughlin (1991) removed the Saffman's restriction on the relative sizes of the two Reynolds numbers. They evaluated the migration velocity as a function of the slip parameter $\alpha = R_s/R_G^{1/2}$. The velocity is maximum in the strong shear case when $\alpha \ll 1$, and is very small, of order $\alpha^{-5}\ln\alpha$, in the opposite weak-shear limit, $\alpha \gg 1$. A recent review of the papers dealing with the inertial lift for non-neutrally buoyant (and neutrally buoyant) particles can be found in Feuillebois (2004).

A detailed analytical study of the structure of the disturbance field in a shear flow is not available yet, except for a single result by McLaughlin (1993), who found that for the inviscid region the velocity in the direction of the shear-rate gradient (normal velocity) decays with the distance from the sphere in the same direction like $r^{-5/3}$ as $r \gg L_S$. Thus the decay in the inviscid region of the shear flow is slower than the r^{-2} decay obtained in uniform flow. This result was used to evaluate the effect of a distant rigid wall on the lift force.

It is important to know not only the normal velocity, but all velocity components over the entire outer region when determining the interaction between sedimenting particles in a dilute dispersion. The inertial interaction of particles in a uniform undisturbed flow, when the outer flow is governed by Oseen solution, was studied by Vasseur & Cox (1977). The particles attract when they are placed in line and the trailing sphere is in the wake of the leading one. They repel for other positions. The mean drag force on the two spheres is reduced for all relative positions. The related case in which both particles are located within each other's inner region of expansion in low Reynolds number was considered by Kaneda & Ishii (1982). Their solution assumes that the distance between sphere centres is large compared with their radii. They also found an attraction between equal spheres moving along their line of centres.

Considerable recent attention has been focussed on a related problem, namely, the inertial effects and particle interactions for neutrally buoyant spheres (Lin, Peery & Schowalter 1970; Poe & Acrivos 1975; Mikulencak & Morris 2004; Matas *et al.* 2004; Subramanian & Koch 2006; Kulkarni & Morris 2008). Lin *et al.* (1970) evaluated the

disturbance velocity to $O(R_G^{3/2})$ in the inner region, $r \ll L_S$, and its effect in suspension rheology. Subramanian & Koch (2006) showed that small fluid inertia breaks the closed-streamline configuration in the near region of a neutrally buoyant sphere predicted in the inertialess limit. As a result, the streamlines are spiralling outward rather than closed. The flows at finite Reynolds numbers were computed using the finite-element (Mikulencak & Morris 2004) and the lattice-Boltzmann (Kulkarni & Morris 2008) methods. The formation of particle chains in dilute suspension flows due to inertial hydrodynamic interactions was observed experimentally (Matas *et al.* 2004). Kulkarni & Morris (2008) obtained numerically reversing and spiralling trajectories of interacting particle pair in finite-inertia shear flow.

Note that the effect of a point force in the outer region exceeds that of a dipole (neutrally buoyant particle) even for a small slip velocity. The disturbance velocity induced by the dipole is (Schonberg & Hinch 1989; Asmolov 1999)

$$u_{nb} \sim GaR_G \quad \text{as} \quad r \ll L_S. \tag{1.2}$$

It can be seen from (1.1) and (1.2) that $u_{nnb} \gg u_{nb}$ when $R_s \gg R_G^{3/2}$, or equivalently, $\alpha \gg R_G$. For the strong shear case, flow disturbances due to the point force dominate, provided $R_G \ll \alpha \ll 1$.

This situation in which $R_s \gg R_G^{3/2}$ is typically applicable to non-neutrally buoyant particles in a vertical shear flow. Note that using the settling Stokes velocity for V_s, this condition gives an upper bound for G, say G_{max} that is independent of the sphere radius a. For instance, for water droplets in air (assuming here a no-slip condition on these droplets), the upper bound is $G_{max} = 5700\,\mathrm{s}^{-1}$ and for particles with mass density 2×10^3 kg m^{-3} in water, $G_{max} = 170\,\mathrm{s}^{-1}$. Thus, most physically relevant cases are concerned.

This work calculates the disturbance velocity induced by a non-neutrally buoyant particle in an unbounded shear flow, including the inviscid region and the viscous wakes. The method of matched asymptotic expansions with a small parameter

$$\varepsilon = R_G^{1/2} = a\,(G/\nu)^{1/2} \ll 1$$

is applied to solve the Oseen-like equations governing the disturbance flow.

The paper is organized as follows. The solution in the outer region is constructed in § 2 in terms of two-dimensional Fourier transforms. The ordinary differential equations for the Fourier transforms of the normal velocity and vorticity are integrated numerically using the orthonormalization method. Small and large wavenumbers correspond in physical space to the far inviscid region and the viscous region near the sphere, respectively. The contributions of these intervals in the Fourier space are estimated asymptotically. Numerical results and comparison with previous studies are presented in § 3. The interaction of particles in a shear flow is considered in § 4. Finally, the results are summarized in § 5.

2. Disturbance flow

Consider a rigid sphere translating parallel to the streamlines of an unbounded shear flow. A sketch of the flow configuration is shown in figure 1. We use a rectangular coordinate system (x, y, z) with origin at the centre of the sphere. The velocity profile in the absence of the sphere is $(V_s + Gz)\,\boldsymbol{e}_x$. The directions of the x and z axis are chosen so that $V_s > 0$ and $G > 0$. To the leading order in Reynolds number, the particle translates along $\boldsymbol{e}_x$ and its migration velocity due to fluid inertia

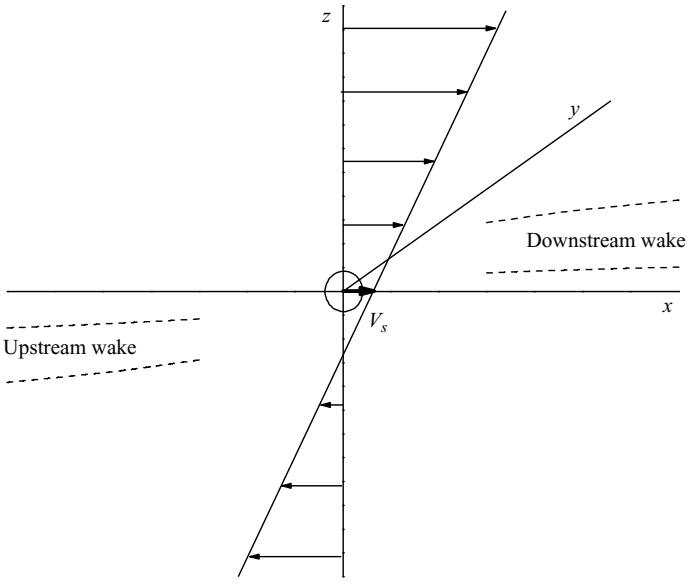

FIGURE 1. Flow configuration in the coordinate system translating with the sphere. Flow disturbances in the outer region are induced by the point force $\boldsymbol{F}$.

is small compared with the slip velocity. As a result, the problem can be treated as quasi-steady. The disturbance velocity $\boldsymbol{u}$ is scaled by the slip velocity V_s, the space coordinates $\boldsymbol{r}$ by the particle radius a and the force on the sphere by $V_s\mu a$.

2.1. *Inner solution*

The dimensionless velocity and pressure fields are sought in the form

$$\boldsymbol{u} = \boldsymbol{u}_0 + \varepsilon \boldsymbol{u}_1 + o(\varepsilon), \quad p = p_0 + \varepsilon p_1 + o(\varepsilon).$$

The axisymmetric leading-order solution decays with the distance from the sphere like r^{-1},

$$\left.\begin{aligned} &\boldsymbol{u}_0 \to \boldsymbol{u}^S \quad \text{as} \quad \boldsymbol{r} \to \infty, \\ &\boldsymbol{u}^S = -\frac{3}{4}\left(\frac{\boldsymbol{e}_x}{r} + \frac{x\boldsymbol{r}}{r^3}\right). \end{aligned}\right\} \tag{2.1}$$

The Stokeslet velocity field $\boldsymbol{u}^S$ corresponds to the viscous flow driven by the point force $\boldsymbol{F} = -6\pi\boldsymbol{e}_x$.

The first-order inner solution $\boldsymbol{u}_1$ does not decay with r, and the boundary condition at infinity has to be replaced by a matching condition with the outer flow. It can be presented in the form (Asmolov 1999)

$$\boldsymbol{u}_1 = \boldsymbol{u}^{nb} + \boldsymbol{u}^{PP} + \boldsymbol{w}. \tag{2.2}$$

Here $\boldsymbol{u}^{nb}$ is the solution of the creeping-flow equations for a force- and torque-free particle in the shear flow. It accounts for the effect of particle rotation. Note that $\boldsymbol{u}^{PP}$ is the first-order inner solution to a uniform undisturbed flow (Proudman &

Pearson 1957):

$$\boldsymbol{u}^{PP} = \frac{3}{32}\alpha\left[\left(2-\frac{3}{r}+\frac{1}{r^2}-\frac{1}{r^3}+\frac{1}{r^4}\right)\left(1-\frac{3x^2}{r^2}\right)\frac{\boldsymbol{r}}{r} + \left(4-\frac{3}{r}+\frac{1}{r^3}-\frac{2}{r^4}\right)\left(\frac{x^2\boldsymbol{r}}{r^3}-\frac{x\boldsymbol{e}_x}{r}\right)\right],$$

$$\alpha = \frac{V_s}{(\nu G)^{1/2}} = \frac{R_s}{R_G^{1/2}} > 0.$$

The third term in (2.2), $\boldsymbol{w}(\boldsymbol{r})$, is a solution to the creeping-flow equations that tends to a uniform flow $\boldsymbol{w}_\infty$ at infinity and satisfies $\boldsymbol{w}=0$ on the particle surface. Here, $\boldsymbol{w}_\infty$ is a migration velocity of an isolated inertialess particle and is found from the matching condition with the outer flow. For an unbounded shear flow, the dependence $\boldsymbol{w}_\infty(\alpha)$ was calculated by Asmolov (1990) and McLaughlin (1991). Because of the symmetry, the regular perturbation expansion (the terms $\boldsymbol{u}^{nb}$ and $\boldsymbol{u}^{PP}$) gives no contribution to the migration velocity. However, the outer limit of $\boldsymbol{u}^{PP}$ is finite

$$\boldsymbol{u}_\infty^{PP} = \boldsymbol{u}^{PP}|_{r\to\infty} = \frac{3}{16}\alpha\left[\left(1-\frac{3x^2}{r^2}\right)\frac{\boldsymbol{r}}{r}+2\left(\frac{x^2\boldsymbol{r}}{r^3}-\frac{x\boldsymbol{e}_x}{r}\right)\right], \tag{2.3}$$

and this term contributes to the outer limit of the inner solution:

$$\boldsymbol{u}_1|_{r\to\infty} = \boldsymbol{u}_\infty^{PP}(\boldsymbol{r}/r) + \boldsymbol{w}_\infty.$$

2.2. *Outer solution*

The outer coordinates are introduced by the scaling $\boldsymbol{R} = (X, Y, Z) = \varepsilon\boldsymbol{r}$. The outer-region velocity and pressure can be presented as

$$\boldsymbol{u} = \varepsilon\boldsymbol{U} + o(\varepsilon), \qquad p = \varepsilon^2 P + o(\varepsilon^2).$$

The outer field, $\boldsymbol{U} = \left(U_x, U_y, U_z\right)$, is governed by the Oseen-like equations:

$$\left.\begin{gathered}\nabla\cdot\boldsymbol{U} = 0,\\ (\alpha+Z)\frac{\partial\boldsymbol{U}}{\partial X} + U_z\boldsymbol{e}_x + \nabla P - \nabla^2\boldsymbol{U} = -6\pi\delta(\boldsymbol{R})\boldsymbol{e}_x,\\ \boldsymbol{U} = 0 \quad \text{as} \quad R\to\infty.\end{gathered}\right\} \tag{2.4}$$

The slip parameter α characterizes the relative sizes of the uniform and shear flows in the undisturbed velocity profile. The effect of the point force on the disturbance flow in the outer region dominates over that of the dipole when $\alpha \gg \varepsilon^2$.

The matching condition with the inner region is

$$\boldsymbol{w}_\infty = \left(\boldsymbol{U}-\boldsymbol{U}^S\right)|_{R\to 0}, \quad \boldsymbol{U}^S = \varepsilon^{-1}\boldsymbol{u}^S.$$

To solve the outer-flow equations, two-dimensional Fourier transforms are introduced by

$$\left\{\begin{matrix}\widetilde{\boldsymbol{U}}\left(k_x,k_y,Z\right)\\ \widetilde{P}\left(k_x,k_y,Z\right)\end{matrix}\right\} = \frac{1}{4\pi^2}\int_{-\infty}^{\infty}\int_{-\infty}^{\infty}\left\{\begin{matrix}\boldsymbol{U}\\ P\end{matrix}\right\}\exp\left[-\mathrm{i}(k_xX+k_yY)\right]\,\mathrm{d}X\,\mathrm{d}Y.$$

The velocity and pressure fields are then expressed as inverse Fourier transforms:

$$\left\{\begin{matrix}\boldsymbol{U}\\ P\end{matrix}\right\} = \int_{-\infty}^{\infty}\int_{-\infty}^{\infty}\left\{\begin{matrix}\widetilde{\boldsymbol{U}}\\ \widetilde{P}\end{matrix}\right\}\exp\left[\mathrm{i}(k_xX+k_yY)\right]\mathrm{d}k_x\,\mathrm{d}k_y. \tag{2.5}$$

The continuity and momentum equations (2.4) are written in terms of the Fourier transforms as

$$\widetilde{\nabla}\cdot\widetilde{\boldsymbol{U}}=0, \tag{2.6}$$

$$\left.\begin{gathered}\mathrm{i}k_x(\alpha+Z)\widetilde{\boldsymbol{U}}+\widetilde{U}_z\boldsymbol{e}_x+\widetilde{\nabla}\widetilde{P}-\widetilde{\Delta}\widetilde{\boldsymbol{U}}=-\frac{3}{2\pi}\delta(Z)\boldsymbol{e}_x,\\ \widetilde{\nabla}=\left(\mathrm{i}k_x,\mathrm{i}k_y,\frac{\mathrm{d}}{\mathrm{d}Z}\right),\quad \widetilde{\Delta}=\frac{\mathrm{d}^2}{\mathrm{d}Z^2}-k^2,\quad k^2=k_x^2+k_y^2.\end{gathered}\right\} \tag{2.7}$$

The equation governing the Fourier transform of the lateral velocity can be derived from (2.6) and (2.7) (Asmolov 1990; McLaughlin 1993):

$$\left.\begin{gathered}\left[\widetilde{\Delta}-\mathrm{i}k_x(\alpha+Z)\right]\widetilde{\Delta}\widetilde{U}_z=-\mathrm{i}k_x\frac{3}{2\pi}\frac{\mathrm{d}\delta(Z)}{\mathrm{d}Z},\\ \widetilde{U}_z\to 0\quad\text{as}\quad Z\to\infty.\end{gathered}\right\} \tag{2.8}$$

The term in the right-hand side of (2.8) is equivalent to a jump condition for the second derivative at the origin of coordinate system

$$\left[\frac{\mathrm{d}^2\widetilde{U}_z}{\mathrm{d}Z^2}\right]=-\mathrm{i}k_x\frac{3}{2\pi}, \tag{2.9}$$

where $[f]=f(+0)-f(-0)$ is the magnitude of the jump.

To obtain equations governing $\widetilde{U}_x$ and $\widetilde{U}_y$, we introduce the Fourier transform of vorticity, $\widetilde{\omega}_z\equiv\mathrm{i}(k_y\widetilde{U}_x-k_x\widetilde{U}_y)$. An equation for $\widetilde{\omega}_z$ can be derived from (2.7):

$$\left[\widetilde{\Delta}-\mathrm{i}k_x(\alpha+Z)\right]\widetilde{\omega}_z=\mathrm{i}k_y\left[\frac{3}{2\pi}\delta(Z)+\widetilde{U}_z\right]. \tag{2.10}$$

The X and Y components of the Fourier transform of the velocity are then expressed, in view of (2.6), in terms of $\frac{\mathrm{d}\widetilde{U}_z}{\mathrm{d}Z}$ and $\widetilde{\omega}_z$ as

$$\widetilde{U}_x=\mathrm{i}k^{-2}\left(k_x\frac{\mathrm{d}\widetilde{U}_z}{\mathrm{d}Z}-k_y\widetilde{\omega}_z\right),\quad \widetilde{U}_y=\mathrm{i}k^{-2}\left(k_y\frac{\mathrm{d}\widetilde{U}_z}{\mathrm{d}Z}+k_x\widetilde{\omega}_z\right). \tag{2.11}$$

Equations (2.8) and (2.10) are integrated numerically using the fourth-order Runge–Kutta routine and the orthonormalization method (Godunov 1961; Conte 1966). The boundaries of the integration domain are set at a sufficiently large distance $|Z|$ from the sphere, so that analytical expressions can be found for linearly independent solutions $\varphi_i(Z)$, $i=1-4$. Small wavenumbers correspond to the velocity field in the far inviscid region. McLaughlin (1993) obtained the asymptotic solution to the Fourier transform of the normal velocity,

$$\left.\begin{gathered}\widetilde{U}_z^{as}=A\,k_x^{2/3}k^{-1}\exp\left(-k\,|Z|\right)\quad\text{as}\quad k\ll 1,\ |Z|\gg 1,\\ \frac{\mathrm{d}\widetilde{U}_z^{as}}{\mathrm{d}Z}=-A\,\mathrm{sgn}\,(Z)\,k_x^{2/3}\exp\left(-k\,|Z|\right),\quad A=\frac{3^{2/3}}{4\pi}\Gamma\left(\frac{2}{3}\right).\end{gathered}\right\} \tag{2.12}$$

He found from (2.12) the asymptotics of the normal velocity on the Z axis:

$$U_z^{as}(0,0,Z)=0.9064\,|Z|^{-5/3}\quad\text{as}\quad |Z|\gg 1. \tag{2.13}$$

Note that U_z^{as} is an even function of Z, i.e. the disturbances are antisymmetric in contrast to the symmetric disturbances in the uniform flow. Assuming, more generally,

$\varphi_i = \exp(\lambda_i |Z|^{\nu_i})$, one can obtain for $\widetilde{U}_z$ two solutions decaying with $|Z|$ (Asmolov 1999):

$$\varphi_1 \sim \exp\left(-k|Z|\right),\ \varphi_2 \sim \exp\left(-\frac{2}{3}\sqrt{\mathrm{i}k_x}\,|Z|^{3/2}\right) \quad \text{as} \quad Z \to \infty,\ k = O(1), \tag{2.14}$$

where the branch of $\sqrt{\mathrm{i}k_x}$ is chosen with a positive real part. So the length scales of the two solutions are $L_1 = k^{-1}$ and $L_2 = |k_x|^{-1/3}$.

The disturbance velocity is found by numerical integration of the inverse Fourier transform (2.5), using plane polar coordinates $k,\ \theta = \arccos(k_x/k)$,

$$\boldsymbol{U} = \int_0^\infty \int_0^{2\pi} \widetilde{\boldsymbol{U}} \exp\left[\mathrm{i}k\left(X\cos\theta + Y\sin\theta\right)\right] k\,\mathrm{d}k\,\mathrm{d}\theta, \tag{2.15}$$

instead of k_x, k_y. It can be seen from (2.8), (2.10) and (2.11) that $\widetilde{U}_z$ and $\widetilde{\boldsymbol{U}}_x$ are even functions of k_y while $\widetilde{\omega}_z$ and $\widetilde{U}_y$ are odd functions. Besides, $\widetilde{\boldsymbol{U}}(k_x, k_y, Z) = \widetilde{\boldsymbol{U}}^*(-k_x, k_y, Z)$, where the superscript $*$ denotes the complex conjugate value. Thus, it is sufficient to integrate (2.5) over the first quadrant:

$$\left.\begin{aligned} U_{x,z} &= 4\int_0^\infty \int_0^{\pi/2} \mathrm{Re}\left[\widetilde{U}_{x,z}\exp\left(\mathrm{i}kX\cos\theta\right)\right]\cos\left(kY\sin\theta\right) k\,\mathrm{d}k\,\mathrm{d}\theta, \\ U_y &= -4\int_0^\infty \int_0^{\pi/2} \mathrm{Im}\left[\widetilde{U}_y\exp\left(\mathrm{i}kX\cos\theta\right)\right]\sin\left(kY\sin\theta\right) k\,\mathrm{d}k\,\mathrm{d}\theta. \end{aligned}\right\} \tag{2.16}$$

These last equations also mean that U_z and U_x are even functions of Y while U_y is an odd function. For the case $\alpha \ll 1$ (the Saffman strong shear limit), the x and z components of the disturbance velocity are also even while the y component is odd in $\boldsymbol{R}$, viz. $U_{x,z}(\boldsymbol{R}) = U_{x,z}(-\boldsymbol{R}),\ U_y(\boldsymbol{R}) = -U_y(-\boldsymbol{R})$. This can be proved if one changes the coordinate system, $\boldsymbol{R}' = (X', Y', Z') = -(X, Y, Z)$, $(k_x', k_y', Z') = -(k_x, k_y, Z)$ and the sign of the point force. Then we have from (2.8), (2.10), (2.11) and (2.16): $\widetilde{\boldsymbol{U}}' = -\widetilde{\boldsymbol{U}}^*$ and $U_{x,z}'(\boldsymbol{R}') = -U_{x,z}(\boldsymbol{R}),\ U_y'(\boldsymbol{R}') = U_y(\boldsymbol{R})$. Note that the disturbance flow induced by a neutrally buoyant particle has another symmetry: U_x' and U_z' are odd in $\boldsymbol{R}$, viz. $U_{x,z}'(\boldsymbol{R}) = -U_{x,z}'(-\boldsymbol{R})$ (Lin *et al.* 1970).

2.3. *Asymptotics of Fourier transforms and inverse integrals for $k \ll 1$ and $k \gg 1$*

The inverse Fourier integrals (2.16) are integrated numerically for a given R up to the wavenumber $k_{max} = 30R^{-1}$. To find the contribution of the interval (k_{max}, ∞), we estimate the integral remainders asymptotically. Moreover, asymptotic solutions to the Fourier transforms for $k \ll 1$ and $k \gg 1$ are required, since the numerical integration of the finite-difference version of ordinary differential equations (2.8) and (2.11) presents some difficulty in these limiting cases. For small k, the two length scales of the two decaying solutions (2.14), L_1 and L_2, are large and they differ significantly, $L_2 \ll L_1$ as $k_x \sim k_y \sim k \ll 1$. The second solution decays faster with Z, so that the first one is dominant in the far region. For this reason, even the orthonormalization technique is not sufficient to give an accurate numerical solution, and an asymptotic solution for $\widetilde{\boldsymbol{U}}$ should be constructed.

The asymptotic solution (2.12) of type φ_1 in (2.14) does not satisfy the jump condition at the origin (2.9), since it is of order $\varphi_1 = O(k^{-1/3})$ giving $[\mathrm{d}^2\varphi_1/\mathrm{d}Z^2] \sim k^{-1/3}L_1^{-2} = O(k^{5/3})$, that is much less than the $O(k)$ required by (2.9). We may thus expect that this jump condition would be satisfied by the second part of the solution in (2.14), provided $[\mathrm{d}^2\varphi_2/\mathrm{d}Z^2] \sim \varphi_2 L_2^{-2} = O(k)$. This yields an estimation for

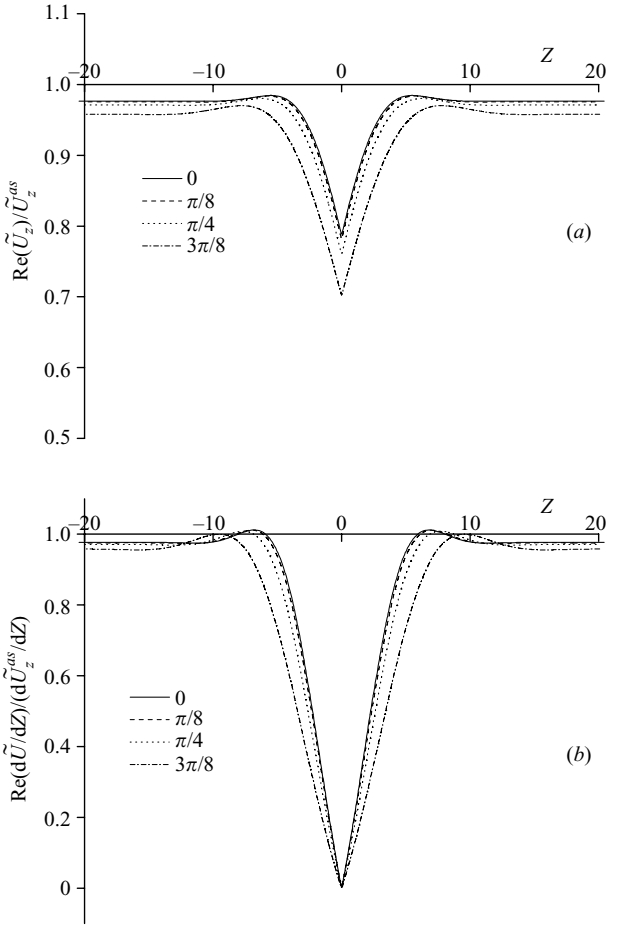

FIGURE 2. Ratios of (*a*) the numerical solution $\widetilde{U}_z$ and (*b*) its derivative to the asymptotic values (2.12), as functions of Z for $k=0.1$, $\alpha \ll 1$ and various θ.

$\varphi_2 = O(k^{1/3}) \ll \varphi_1$. This result says that McLaughlin's solution (2.12) is the dominant one, provided $k \ll 1$.

This is checked by comparing the numerical solution of (2.8) with (2.12) at small k. The integration of (2.8) is fulfilled up to $|Z| = 20L_1$. Figure 2 shows the results of the calculation of the ratios $\mathrm{Re}(\widetilde{U}_z)/\widetilde{U}_z^{as}$ and $\mathrm{Re}(\mathrm{d}\widetilde{U}_z/\mathrm{d}Z)/(\mathrm{d}\widetilde{U}_z^{as}/\mathrm{d}Z)$ at $k=0.1$, $\alpha \ll 1$ and various $\theta = 3\pi/8,\ \pi/4,\ \pi/8,\ 0$. It can be seen that the numerical solution is close to the asymptotic one for $|Z| \sim k^{-1}$ as $k \ll 1$. The deviation of the first derivative from the asymptotic value is greater.

Important features of U_z in the far inviscid region can be found from (2.12). The velocity field at large R is due to small k. The McLaughlin's power law for the normal velocity (2.13) can then be readily derived from the scaling of the Fourier transform $\widetilde{U}_z^{as} \sim k^{-1/3}\exp(-k\,|Z|)$. Small wavenumbers, $k \sim |Z|^{-1} \ll 1$, contribute to (2.16), and $U_z \sim \widetilde{U}_z k^2 \sim |Z|^{-5/3}$ at $|Z| \gg 1$. Substituting (2.12) into (2.5) one has

$$U_z = A\int_{-\infty}^{\infty}\int_{-\infty}^{\infty} k_x^{2/3}k^{-1}\exp\left[-k\,|Z| + \mathrm{i}\left(k_x X + k_y Y\right)\right]\mathrm{d}k_x\,\mathrm{d}k_y \quad \text{as} \quad R \gg 1.$$

Integrating the last equation over k_y yields

$$U_z = 2A \int_{-\infty}^{\infty} \mathrm{K}_0 (k_x \rho)\, k_x^{2/3} \exp(\mathrm{i} k_x X)\, \mathrm{d}k_x \quad \text{as} \quad \rho \gg 1, \tag{2.17}$$

where $\rho = (Y^2 + Z^2)^{1/2}$ and K_0 is the modified Bessel function. Equation (2.17) means that for large ρ the U_z field has a cylindrical symmetry, $U_z = U_z(X, \rho)$, for arbitrary α and X. When $X = 0$, the integration over k_x can also be fulfilled in (2.17) (Abramowitz & Stegun 1964):

$$U_z = 2^{4/3} A\, (\Gamma(5/6))^2\, \rho^{-5/3} = 0.9064 \rho^{-5/3} \quad \text{as} \quad X = 0, \ \rho \gg 1. \tag{2.18}$$

Thus, we extend the asymptotic result (2.13), obtained by McLaughlin for the Z axis only ($X = 0, \ Y = 0$), to the median plane, $X = 0$. The disturbance decays like $\rho^{-5/3}$ in the median plane of the inviscid region in a shear flow, which is slower than the ρ^{-2} decay of disturbances in a uniform flow.

An asymptotic solution can also be obtained for the Fourier transform of the vorticity, $\widetilde{\omega}_z$, as $|Z| \sim k^{-1} \gg 1$. The term proportional to $\widetilde{U}_z \sim k^{-1/3} \gg 1$ in the right-hand side of (2.10) is the only left one, since the δ function vanishes for $Z \neq 0$. Since $|\widetilde{\Delta}| \sim k^2 \ll |k_x (\alpha + Z)| \sim 1$, the asymptotic result for (2.10) is, using also (2.12)

$$-\mathrm{i} k_x Z \widetilde{\omega}_z^{as} = \mathrm{i} k_y \widetilde{U}_z = \mathrm{i} A k_x^{2/3} k_y k^{-1} \exp(-k|Z|) \quad \text{as} \quad |Z| \sim k^{-1} \gg 1. \tag{2.19}$$

In view of (2.11), (2.12) and (2.19), the asymptotic solutions for $\widetilde{U}_x$ and $\widetilde{U}_y$ at $|Z| \sim k^{-1} \gg 1$ are

$$\left.\begin{aligned} \widetilde{U}_x &= \frac{\mathrm{i}A}{k_x^{1/3} k^2} \left(-\mathrm{sgn}(Z)\, k_x^2 + \frac{k_y^2}{Zk} \right) \exp(-k|Z|), \\ \widetilde{U}_y &= \frac{\mathrm{i}A k_x^{2/3} k_y}{k^2} \left(-\mathrm{sgn}(Z) - \frac{1}{Zk} \right) \exp(-k|Z|). \end{aligned}\right\} \tag{2.20}$$

The plots of the numerical solution $\widetilde{\omega}_z$ multiplied by $\exp(k|Z|)$ and the asymptotic solution following from (2.19), $\widetilde{\omega}_z^{as} \exp(k|Z|) = -A k_x^{-1/3} k_y k^{-1} Z^{-1}$, are compared in figure 3 for $k = 0.1$, $\alpha \ll 1$ and $\theta = 3\pi/8$. We have again a good agreement for large Z, but for $Z = O(1)$ the difference is significant, since the asymptotic solution grows like Z^{-1} as $Z \to 0$. The comparison shows that the numerical integration of (2.8) and (2.10) can be fulfilled within a smaller interval, say, $-20L_2 \leqslant Z \leqslant 20L_2$. For larger $|Z|$, the asymptotic solutions (2.12) and (2.20) are used.

At large wavenumbers, the obtained numerical solution is close to the two-dimensional Fourier transforms of the Stokeslet and Oseenlet,

$$\widetilde{\boldsymbol{U}} = \widetilde{\boldsymbol{U}}^S \left[1 + O\left(k^{-1}\right)\right], \quad \widetilde{\boldsymbol{U}} = \widetilde{\boldsymbol{U}}^O \left[1 + O\left(k^{-2}\right)\right] \quad \text{as} \quad k \gg 1.$$

Here, $\widetilde{\boldsymbol{U}}^S$ and $\widetilde{\boldsymbol{U}}^O$ are (Vasseur & Cox 1977)

$$\begin{aligned} \widetilde{U}_x^S &= \frac{3}{8\pi} \left[-\frac{2}{k} + \frac{k_x^2}{k^3} (1 + k|Z|) \right] \exp(-k|Z|), \\ \widetilde{U}_y^S &= \frac{3}{8\pi} \frac{k_x k_y}{k^3} (1 + k|Z|) \exp(-k|Z|), \\ \widetilde{U}_z^S &= \frac{3}{8\pi} \frac{\mathrm{i} k_x}{k} Z \exp(-k|Z|), \end{aligned}$$

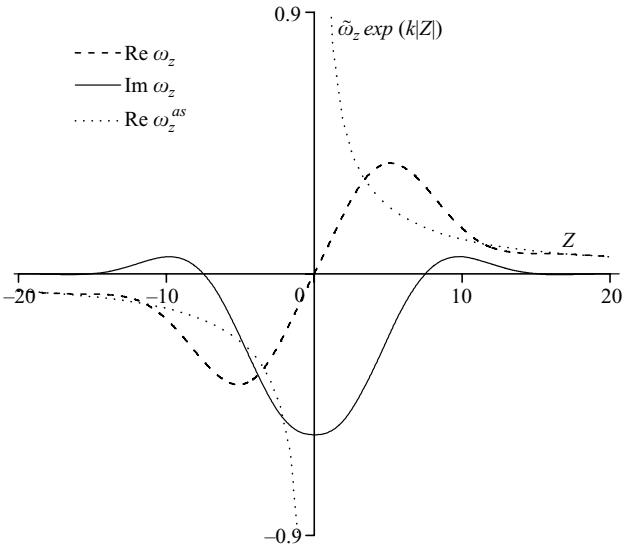

FIGURE 3. Numerical solution for the Fourier transform of vorticity $\widetilde{\omega}_z$ multiplied by $\exp(k|Z|)$, in comparison with the asymptotic solution following from (2.19) for $k=0.1$, $\alpha \ll 1$ and $\theta = 3\pi/8$.

$$\widetilde{U}_x^O = -\frac{3}{4\pi\alpha}\left[\frac{\mathrm{i}k_x \exp(-k|Z|)}{k} - \frac{(\mathrm{i}k_x-\alpha)\exp(-t|Z|)}{t}\right],$$

$$\widetilde{U}_y^O = -\frac{3\mathrm{i}k_y}{4\pi\alpha}\left[\frac{\exp(-k|Z|)}{k} - \frac{\exp(-t|Z|)}{t}\right],$$

$$\widetilde{U}_z^O = \frac{3}{4\pi\alpha}\mathrm{sgn}(Z)\left[\exp(-k|Z|) - \exp(-t|Z|)\right],$$

$$t = \sqrt{k^2 + \mathrm{i}\alpha k_x}.$$

A large k corresponds to the velocity field in the viscous region. When $|Z| \sim R \ll 1$, a dominant contribution to the integral (2.16) over the k space comes from the values $k \sim R^{-1}$. As a result, $\boldsymbol{U} \sim \widetilde{\boldsymbol{U}} k^2 \sim R^{-1}$ and the solution matches with the Stokeslet $\boldsymbol{U}^S = \varepsilon^{-1}\boldsymbol{u}^S$.

The difference between the numerical and Stokeslet Fourier transforms, $\widetilde{\boldsymbol{U}} - \widetilde{\boldsymbol{U}}^S$, corresponds to the first-order velocity field (2.2). Its integral over large $k = O(R^{-1})$ provides the discontinuity $\boldsymbol{u}_1$ at the origin given by $\boldsymbol{u}_\infty^{PP}$. The uniform flow, $\boldsymbol{w}_\infty$, matches with the inner limit of $\boldsymbol{U} - \boldsymbol{U}^O$,

$$\boldsymbol{w}_\infty = \left\{\int\int\left(\widetilde{\boldsymbol{U}} - \widetilde{\boldsymbol{U}}^O\right)\exp\left[\mathrm{i}k\left(X\cos\theta + Y\sin\theta\right)\right]k\,\mathrm{d}k\,\mathrm{d}\theta\right\}\Big|_{R\to 0}. \tag{2.21}$$

To estimate the asymptotic contribution of the interval (k_{max}, ∞) to the inverse-Fourier integral (2.15) for the domain $k_{max}|Z| \gg 1$, one can present the Fourier transform in the form $\widetilde{\boldsymbol{U}} = \boldsymbol{a}(k,\theta,Z)\exp(-k|Z|)$, where the vector $\boldsymbol{a}$ does not contain exponential functions of the large parameter. Then one has, for $S = O(1)$

(Sidorov, Fedoryuk & Shabunin 1976):

$$\int_{k_{max}}^{\infty} \boldsymbol{a} \exp(-kS)\, k\, \mathrm{d}k$$
$$= \frac{\boldsymbol{a}(k_{max}, \theta, Z)\, k_{max} \exp(-k_{max} S)}{S} \left[1 + O\left(\frac{1}{k_{max} R}\right)\right] \quad \text{as} \quad k_{max} R \gg 1,$$

$$S = |Z| - \mathrm{i}(X \cos\theta + Y \sin\theta), \quad S = O(R).$$

The main contribution to the integral over θ comes from small intervals near the points $\theta_0 = \arctan(Y/X) \pm \pi$ where $\mathrm{Re}\, S$ is minimum. As a result the remainder of the integral (2.15) can be estimated to the leading order as

$$\int_{k_{max}}^{\infty} \int_0^{2\pi} \widetilde{\boldsymbol{U}} \exp[\mathrm{i}k(X \cos\theta + Y \sin\theta)]\, k\, \mathrm{d}k\, \mathrm{d}\theta$$
$$= 2\mathrm{Re}\left[\sqrt{\frac{2\pi k_{max}}{\eta}} \frac{\boldsymbol{a}(k_{max}, \theta_0, Z) \exp\{\mathrm{i}(k_{max}\eta - \pi/4) - k_{max}|Z|\}}{\mathrm{i}\eta - |Z|}\right],$$

where $\eta^2 = X^2 + Y^2$. The above calculations are also valid when $k_{max}|Z| \sim 1$ but $k_{max} R \gg 1$.

3. Numerical results

The inertial migration velocity calculated using (2.21) coincides for $\alpha \ll 1$ with the values obtained previously: $w_{z\infty} = 0.343$ (Saffman 1965, 1968) and $w_{x\infty} = 0.0735$ (Miyazaki *et al.* 1995). The Ycomponent of the migration velocity is zero since U_y is an odd function of Y.

The normal velocity field U_z is illustrated in figures 4–6. Since the Stokeslet velocity U_z^S is zero at $X = 0$, by matching the function U_z has finite inner limits ($X \to 0$) along the Y and Z axes. Figure 4 shows $U_z(0, 0, Z)$ for values of $\alpha \ll 1$, $\alpha = 1$ and $\alpha = 2$. The uniform part of the flow $\boldsymbol{w}_\infty(\alpha)$ at the origin given by (2.21) (shown by dots in figure 4*a*) coincides with the results of Asmolov (1990) and McLaughlin (1991). It is the normal migration velocity of an isolated particle. The numerical values of the jump at the origin agree with the discontinuity predicted by $\boldsymbol{u}_\infty^{PP}$. For large $|Z|$, the function follows the $|Z|^{-5/3}$ power law (see figure 4*b*) in accordance with McLaughlin's solution (2.13).

Figure 5 presents U_z as a function of Y for the same values α and $X = Z = 0$. For large Y, all curves are close to the asymptotic solution $0.9064|Y|^{-5/3}$ (see (2.18)). The cylindrical symmetry of U_z for large R following from (2.17) is illustrated in figure 6.

Figure 7 shows the Y component of the disturbance velocity as a function of Y for $X = Z = 0$. Note that U_y is zero for $\alpha \ll 1$ because of the symmetry. The results are compared with the transversal disturbance velocity in the uniform flow (Vasseur & Cox 1977),

$$U_\perp^{VC} = \frac{3}{4\alpha R^2}(2 - (R\alpha + 2)\exp(-R\alpha/2)). \tag{3.1}$$

The disturbances in the shear flow are always larger. Both dependences give the same limit $U_y|_{Y\to 0} = 3\alpha/16\ \mathrm{sgn}(Y)$ matching the first-order outer limit of the inner solution (2.3). Note that $U_\perp^{VC}$ decays like R^{-2} in the inviscid region. It is seen in figure 7(*b*) that U_y decays very slowly, like $|Y|^{-4/3}$, at large distances.

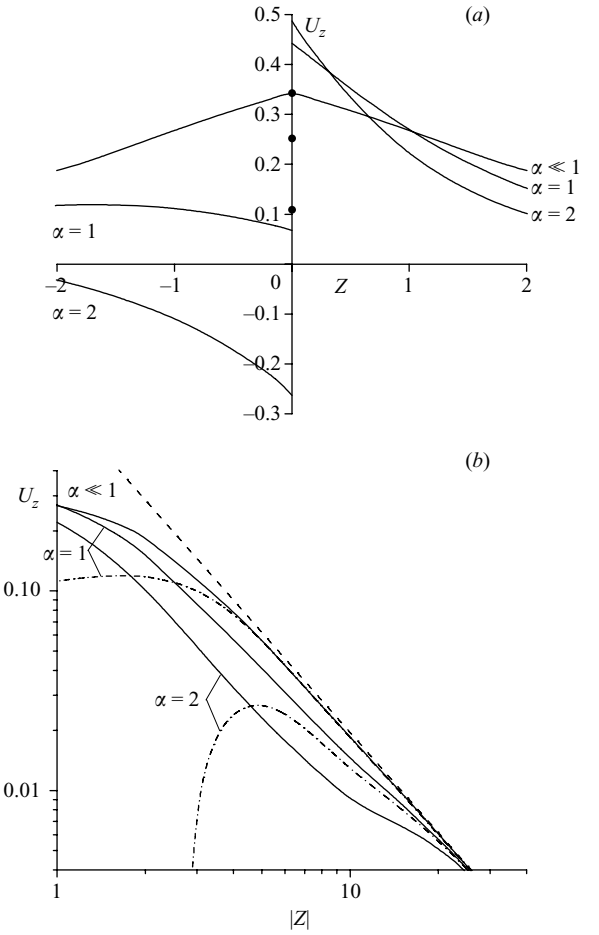

FIGURE 4. U_z as a function of Z for $X = Y = 0$ at (a) finite and (b) large distances. In (a), the dots represent $\boldsymbol{w}_\infty$, (2.21). In (b), the solid and dash-dotted lines correspond to $Z > 0$ and $Z < 0$, respectively. The dashed line is Mclaughlin's asymptotic solution, $U_z^{as} = 0.9064\,|Z|^{-5/3}$.

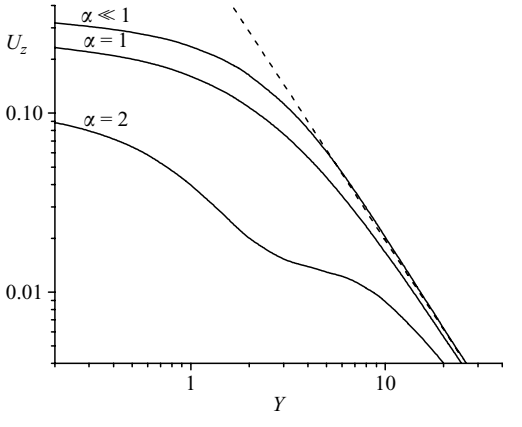

FIGURE 5. U_z as a function of Y for $X = Z = 0$. For other symbols, see figure 4.

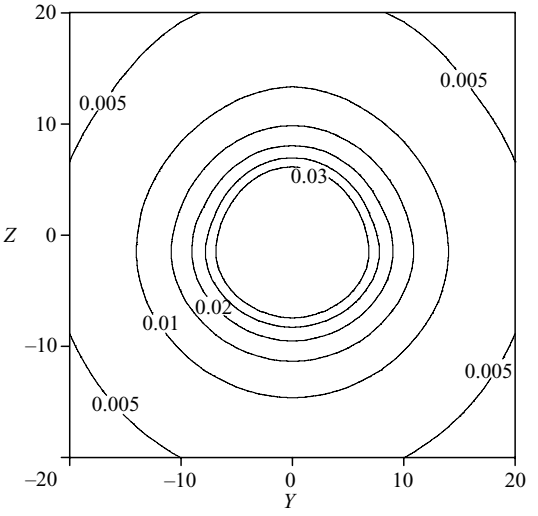

FIGURE 6. Isolines of U_z for $X = 0$, $\alpha = 1$. This velocity component is nearly cylindrically symmetric at large distances.

Figures 8 and 9 show the isolines of U_y and the (U_y, U_z) vector field in the median plane $X = 0$. The U_y field in contrast to U_z component is elongated in the transverse direction.

Figures 10–12 present U_x as functions of Z, Y and X on the three coordinate axes, respectively. The X component of disturbance velocity is close to the Stokeslet, ((2.1), dotted lines), at small distances. It changes sign far from the particle, at $X = Y = O$, $Z = O(10)$. For large Z, the dominant contribution to U_x comes again from small $k \sim |Z|^{-1}$ where the asymptotic solution (2.20) is valid. However, the solution for $\widetilde{U}_x$, unlike $\widetilde{U}_z$, is purely imaginary and hence does not contribute to (2.16). As a result, $U_x(0, 0, Z)$ decays faster than $|Z|^{-2}$. The Y dependence of the longitudinal disturbance velocity also decays fast. Thus, U_x is smaller than the other velocity components in the median plane of the inviscid region, $R \gg 1$. However, it is the largest one within the viscous wakes as shown below.

3.1. *Wakes in a linear shear flow*

A non-neutrally buoyant particle produces in the surrounding fluid a momentum deficit equal to its drag. The region of reduced momentum is advected by the undisturbed shear flow and grows diffusively. A wake is due to a balance of the two processes. For a uniform Oseen flow, the time taken to travel from the particle to some downstream position x' is $t^O = x'/V_s$, where the prime denotes dimensional coordinates. During this time the deficit diffuses in normal direction to a distance $z'^O_w \sim (\nu t^O)^{1/2}$, so the wake width varies like $z'^O_w \sim (\nu x'/V_s)^{1/2}$. In a linear shear flow, the momentum deficit is advected both downstream and upstream, and two wakes arise (see figure 1). The formation of two wakes in a shear flow was predicted earlier for neutrally buoyant particles (Subramanian & Koch 2006). It should be noted that the two cases differ significantly. As a neutrally buoyant particle is force-free, no momentum deficit but the vorticity only is advected in the wakes. That case is analogous in the limit of a point particle to the diffusion problem from a point source in shear flow which was solved analytically by Elrick (1962). The flow symmetries are

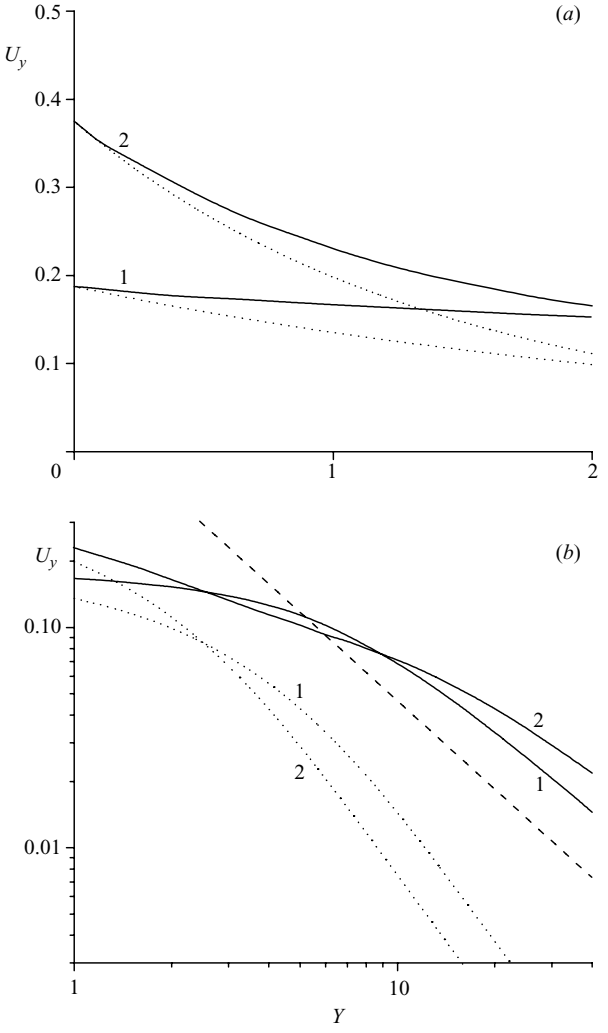

FIGURE 7. U_y as a function of Y for $X = Z = 0$ at (a) finite and (b) large distances. Numbers on the curves are the values of α. Dotted lines represent the relationships (3.1) for the uniform undisturbed flow (Vasseur & Cox 1977), dashed line is $Y^{-4/3}$.

also different: $U_{x,z}(\boldsymbol{R}) = U_{x,z}(-\boldsymbol{R})$ for the flow due to the point force in the strong shear limit and $U_{x,z}(\boldsymbol{R}) = -U_{x,z}(-\boldsymbol{R})$ for the flow induced by the dipole.

For $\alpha \ll 1$, the advection speed is Gz' and the wakes are antisymmetric. When $X = O(1)$ the maximum disturbance velocity is on the X axis. The dash-double-dotted (maximum velocity for $\alpha \ll 1$) and solid (velocity at $Y = Z = 0$ for $\alpha \ll 1$) lines in figure 12 coincide up to $|X| \simeq 3$. For larger X the two lines diverge, and the maximum of U_x is away from the X axis, i.e. the wake core is in the region where the advection speed is large. Balancing a time z'^2/ν to diffuse to z' and a time x'/Gz' to travel to x' provides the wake width $z'^{sh}_w \sim (\nu x'/G)^{1/3}$, or in terms of stretched coordinates $Z^{sh}_w \sim X^{1/3}$. The diffusion occurs in both the Z and Y directions; hence, the wake width in both directions is the same, $Y^{sh}_w \sim Z^{sh}_w$.

The momentum flux across the wake cross-section is constant for a uniform undisturbed flow, from Oseen's equation: $\int V_s U'_x \, \mathrm{d}y' \, \mathrm{d}z' \sim V_s U'_x (z'^O_w)^2 = 6\pi\nu a V_s$. This

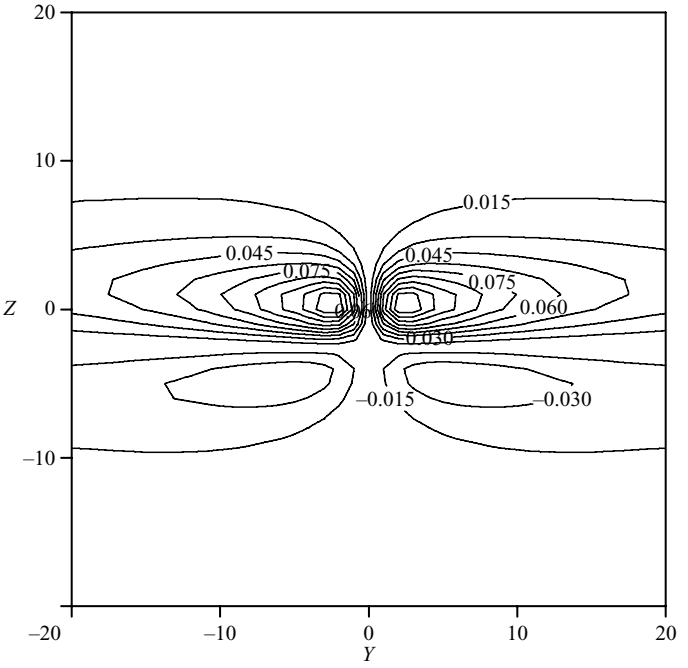

FIGURE 8. Isolines of U_y at $X = 0$, $\alpha = 1$.

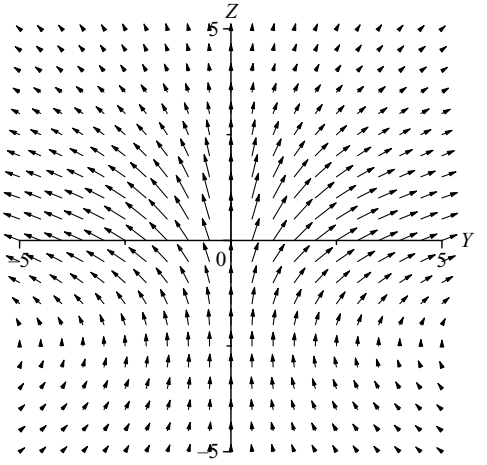

FIGURE 9. Vector field (U_y, U_z) at $X = 0$, $\alpha = 1$.

gives the scaling for the velocity disturbance, $U_x' \sim V_s a/x'$. Now for a shear flow, our numerical calculations show that the maximum velocity in the wake (dash-double-dotted line in figure 12) decays at $\alpha \ll 1$ like $X^{-2/3}$. The deficit is advected away from the particle in two quadrants only, $X > 0$, $Z > 0$ and $X < 0$, $Z < 0$. In the other two quadrants the radial undisturbed velocity is negative. Streamlines come there from infinity where disturbances are zero. The momentum is transferred into these regions because of normal diffusion only. Then it is advected towards the sphere by the reverse flow, and hence the momentum flux across the wake is not constant. Figure 13(*a*)

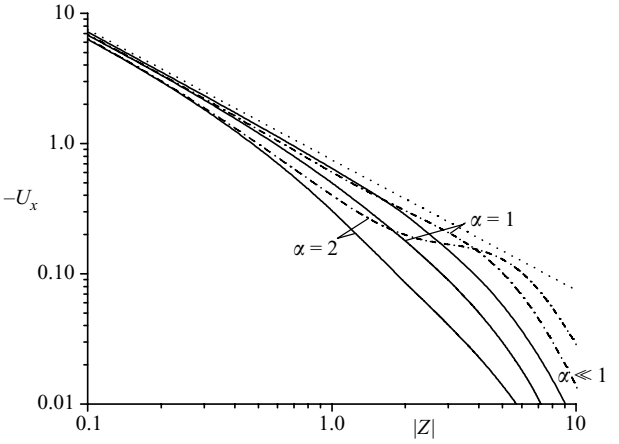

FIGURE 10. U_x as a function of Z for $X = Y = 0$. Dotted line is the Stokeslet. For other symbols, see figure 4.

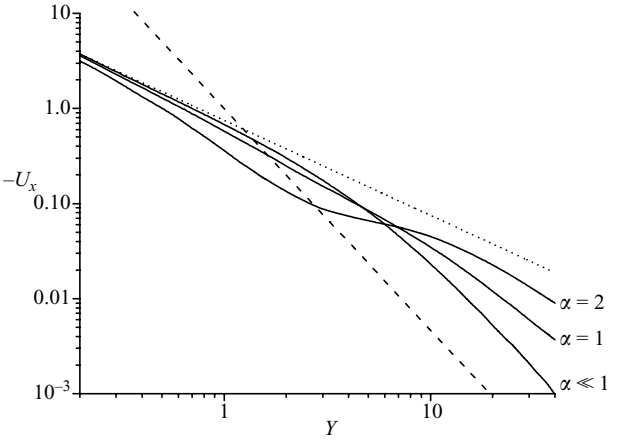

FIGURE 11. U_x as a function of Y for $X = Z = 0$. Dotted and dashed lines are the Stokeslet and $Y^{-7/3}$, respectively.

shows the profiles of U_x scaled by $X^{-2/3}$ as functions of $ZX^{-1/3}$ for $\alpha \ll 1$, $Y = 0$. The profiles calculated for different X are close near the wake cores and large positive Z. However, in the reverse-flow region ($ZX^{-1/3} < 0$) and in the intermediate domain near the X axis, the profiles differ significantly. The normal velocity decays in the wake core like X^{-1} (see figure 13*b*).

For $\alpha > 0$ the wake is asymmetric. Figure 14 shows the vector field in far (*a*) upstream and (*b*) downstream regions at $Y = 0$, $\alpha = 1$. The greater portion of the deficit is in the downstream wake where $Z > 0$ since the advection speed $Z + \alpha$ is greater there. The wake core is closer to the X axis. For the upstream wake, it is farther away since on the axis the undisturbed flow is directed towards the sphere. Figure 15 shows the velocity profiles U_x and U_z for $\alpha = 1$, $Y = 0$. In this case U_x and U_z also decay approximately like $X^{-2/3}$ and X^{-1} respectively, especially in the upstream wake.

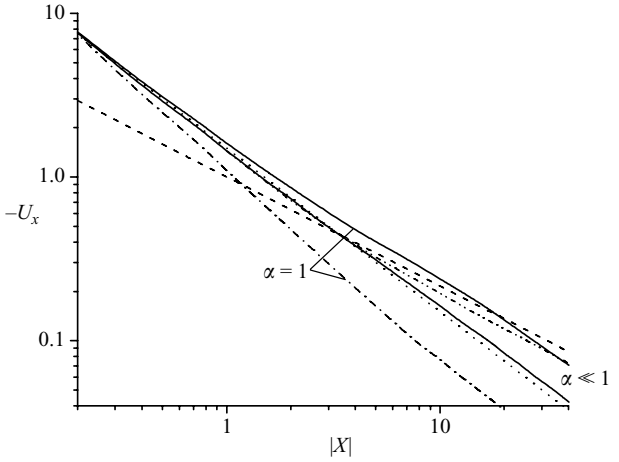

FIGURE 12. U_x as a function of X for $Y = Z = 0$. Dotted and dashed lines are the Stokeslet and $X^{-2/3}$, respectively. Dash-double-dotted line is the maximum velocity in the wake core for $\alpha \ll 1$. For other symbols, see figure 4.

4. Inertial interaction of two particles

The presented detailed knowledge of the disturbance flow past a single sphere enables us to consider now the interaction of two particles in a shear flow. The inertial interaction of particles was studied earlier by Vasseur & Cox (1977) for a uniform undisturbed flow, when the outer flow is governed by Oseen solution. The drag on the trailing sphere is less than if isolated, since it lies in the wake induced by the leading one. Thus particles attract in a uniform flow. For neutrally buoyant particles, inertial hydrodynamic interactions result in particle attraction and formation of particle chains in dilute suspension shear flows (Matas *et al.* 2004; Kulkarni & Morris 2008).

Two rigid spheres A and B, centred at the origin and at $\boldsymbol{R}_B$ respectively, are assumed to move in the X direction. The distance $|\boldsymbol{R}_B|$ is assumed to be large enough for each sphere to be in the Saffman's region of the other sphere. The dimensionless momentum equation governing the flow in the outer region can be written as

$$\frac{\partial \boldsymbol{U}}{\partial t} + (\alpha_A + Z)\frac{\partial \boldsymbol{U}}{\partial X} + U_z \boldsymbol{e}_x + \nabla P - \nabla^2 \boldsymbol{U} = -\left[F_A \delta(\boldsymbol{R}) + F_B \delta(\boldsymbol{R} - \boldsymbol{R}_B)\right] \boldsymbol{e}_x.$$

Here, distances are scaled by the Saffman length $L_S = (\nu/G)^{1/2}$. The symbols F_A, F_B denote the forces along $\boldsymbol{e}_x$ exerted on particles A, B, respectively.

To the leading order, the particle B translates in the shear flow relative to A with the velocity

$$\boldsymbol{v}_{0B} = (Z_B/\alpha_A + 1 - V_{sB}/V_{sA})\,\boldsymbol{e}_x,$$

and its position $\boldsymbol{R}_B$ changes with time. Thus, the problem is unsteady unlike that for a single particle. Nevertheless, it can be reduced to the steady one-particle problem. The governing equations are linear and the boundary condition at infinity is again a vanishing disturbance. Hence, the flow can be decomposed into the parts due to the two point forces, $\boldsymbol{U} = \boldsymbol{U}_A(\boldsymbol{R}) + \boldsymbol{U}_B(t, \boldsymbol{R})$. The second part can be evaluated using another coordinate system, with its origin at the centre of the particle B and translating with the velocity $\boldsymbol{v}_{0B}$ relative to the first system. The considered flow

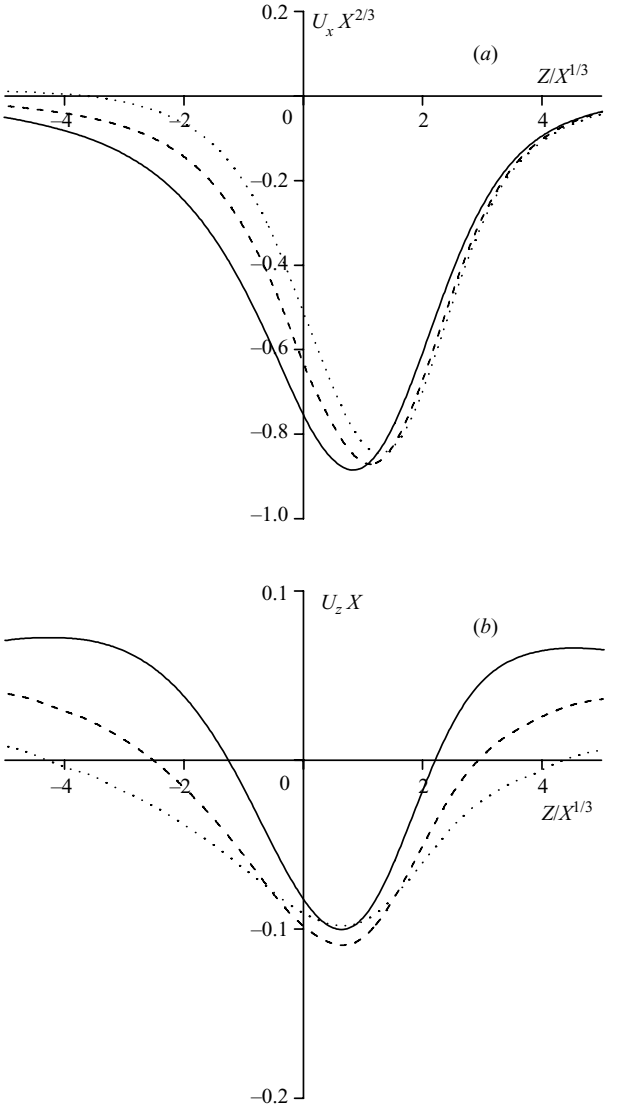

FIGURE 13. (*a*) $U_x X^{2/3}$ and (*b*) $U_z X$ as the functions of $ZX^{-1/3}$ for $\alpha \ll 1$, $Y = 0$ and $X = 10,\ 20,\ 40$ (solid, dashed and dotted lines, respectively).

is then the superposition of the two parts that are quasi-steady in each respective coordinate system: $\boldsymbol{U} = \boldsymbol{U}_A(\boldsymbol{R}) + \boldsymbol{U}_B(\boldsymbol{R} - \boldsymbol{R}_B^0 - \boldsymbol{v}_{0B}t)$ where $\boldsymbol{R}_B^0$ is the initial position of particle B. Thus, to describe the interaction of two particles one should know only the disturbance field $\boldsymbol{U}(\boldsymbol{R})$ induced by an isolated particle.

The migration velocity of each particle is the sum of the velocity due to the effect of the particle itself and of the disturbance flow induced by the other particle,

$$\boldsymbol{v}_{1A} = \boldsymbol{w}_\infty(\alpha_A) + \frac{F_B}{F_A}\boldsymbol{U}(\alpha_B, -\boldsymbol{R}_B), \quad \boldsymbol{v}_{1B} = \frac{F_B}{F_A}\boldsymbol{w}_\infty(\alpha_B) + \boldsymbol{U}(\alpha_A, \boldsymbol{R}_B).$$

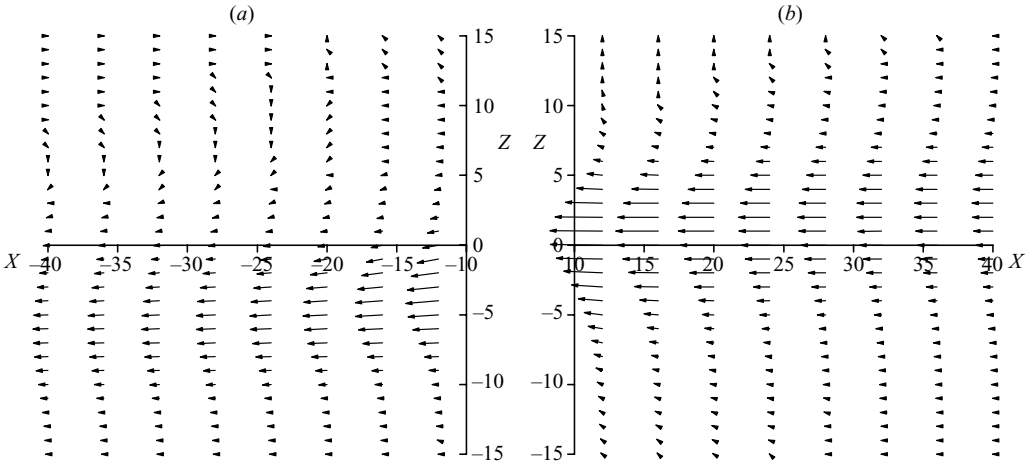

FIGURE 14. Vector field (U_x, U_z) at $Y=0,\ \alpha=1$ in far (a) upstream and (b) downstream regions.

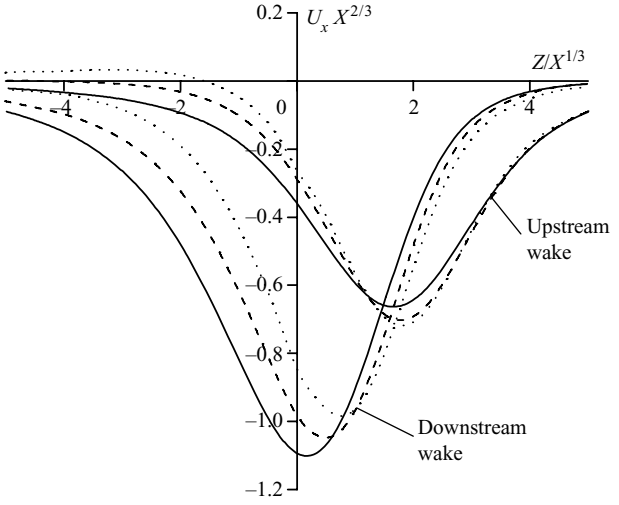

FIGURE 15. Upstream and downstream wakes for $\alpha=1,\ Y=0$. (a) $U_x X^{2/3}$ and (b) $U_z X$ as the functions of $ZX^{-1/3}$ at $X=10,\ 20,\ 40$ (solid, dashed and dotted lines, respectively).

We study in detail the case of equal spheres, $\alpha_A=\alpha_B=\alpha,\ F_A=F_B=6\pi$. Then the rate of particle separation is

$$\Delta \boldsymbol{v} = \boldsymbol{v}_B - \boldsymbol{v}_A = \Delta \boldsymbol{v}_0 + \varepsilon \Delta \boldsymbol{v}_1 + O\left(\varepsilon^2\right),$$
$$\Delta \boldsymbol{v}_0 = \frac{Z_B}{\alpha}\boldsymbol{e}_x, \quad \Delta \boldsymbol{v}_1 = \boldsymbol{U}\left(\alpha, \boldsymbol{R}_B\right) - \boldsymbol{U}\left(\alpha, -\boldsymbol{R}_B\right). \tag{4.1}$$

The undisturbed flow $\Delta \boldsymbol{v}_0$ dominates in the relative motion in the shear flow, and the inertial interaction $\Delta \boldsymbol{v}_1$ gives only a small correction for $Z_B = O(1)$. Note that $\Delta \boldsymbol{v}_1$ becomes important when Z_B is small.

Vasseur & Cox (1977) considered the inertial particle interaction in a uniform undisturbed flow when $\Delta \boldsymbol{v}_0 = 0$. The particles placed in the normal direction with respect to the slip velocity repel. The rate of separation in the normal direction is

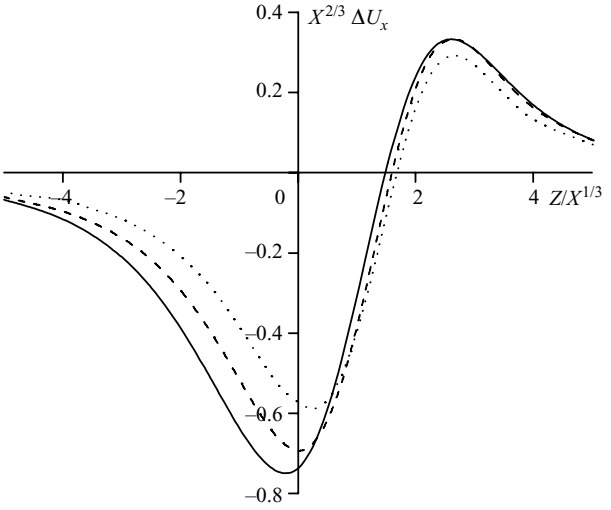

FIGURE 16. $X^{2/3}\Delta v_{1x}$ as a function of $ZX^{-1/3}$ for $\alpha = 1$, $Y = 0$ and $X = 10,\ 20,\ 40$ (solid, dashed and dotted lines, respectively).

$\Delta v_{1\perp}^{VC} = 2U_{\perp}^{VC} > 0$, where $U_{\perp}^{VC}$ is given by (3.1), while other components are zero because of the symmetry. The particles attract when their line of centres is parallel to the slip velocity. The drag on the trailing sphere is less than if isolated, since it lies in the wake induced by the leading one.

For the shear flow, the first-order disturbance field is close to the Oseenlet as $R \ll 1$. As a result, the particle inertial interaction at small separations coincide with the predictions of Vasseur & Cox (1977):

$$\Delta \boldsymbol{v}_1|_{R_B \to 0} = 2\boldsymbol{u}_{\infty}^{PP}.$$

When the particles are placed in the transversal directions, $\boldsymbol{R}_B = (0, Y_B, 0)$, we have $\Delta v_{1y} = 2U_y$ and $\Delta v_{1x} = \Delta v_{1z} = 0$. The particles repel for such relative positions at any Y_B, and their separation rate in the shear flow is always larger than that in the uniform flow (see figure 7).

Consider now two particles aligned along the unperturbed flow. The trailing sphere catches up the leading one at small separations:

$$\Delta v_{1x}\,(X_B, 0, 0)\,|_{X_B \to +0} = 2u_{\infty\parallel}^{PP} = -\frac{3\alpha}{4}.$$

At large distances, two wakes arise around each particle in the shear flow, so that each particle is in the wake of the other one, and $\Delta v_{1x} = U_x^{dw} - U_x^{uw}$ can be either positive or negative. Here U_x^{dw} and U_x^{uw} are the velocities in the downstream and upstream wakes, respectively, shown in figure 15(a). Figure 16 presents $\Delta v_{1x}\,(X_B, 0, Z_B)$, $X_B > 0$, scaled by $X_B^{-2/3}$ as a function of $Z_B X_B^{-1/3}$ for $\alpha = 1$. Near the X axis the rate of separation in the X direction is negative and the two particles attract, similar to the uniform-flow case. However, the particle B starting at the X axis does not meet A since the rate of separation in the Z direction is nonzero for the shear flow, unlike the uniform-flow case. It can be concluded from the results shown in figure 15(b) that $\Delta v_{1z} = U_z^{dw} - U_z^{uw}$ is positive in the wake for any Z_B. The approaching trajectories can be obtained for a finite positive X_B and a small negative Z_B where $\Delta v_{0x} < 0$ (see figure 17). If we assume that $|Z_B| \gg \varepsilon$, the undisturbed flow dominates over the inertial

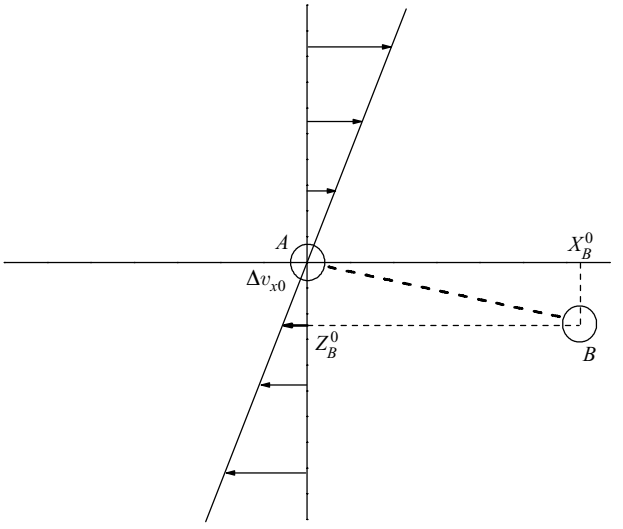

FIGURE 17. Trajectory of particle B attracted by particle A (dashed line) in a shear flow.

interaction Δv_{1x} in the relative motion in the X direction. Then the separations in the X and Z directions on the trajectory can be estimated using (4.1) as

$$X_B \sim -\Delta v_{0x} t_{app} \sim -Z_B t_{app}/\alpha, \quad Z_B \sim -\varepsilon \Delta v_{1z} t_{app} \sim -\varepsilon \alpha X_B t_{app},$$

where t_{app} is the time required for the particles to approach in the outer region. Eliminating t_{app} in these equations, one has

$$Z_B \sim -\varepsilon^{1/2} \alpha X_B = -R_G^{1/4} \alpha X_B.$$

Thus, the particles may approach when their line of centres is nearly parallel to the slip velocity.

5. Conclusions

Comprehensive results are provided for the disturbance flow due to the motion of a small sphere in a linear shear flow. The method of matched asymptotic expansions based on a small particle Reynolds number and the two-dimensional Fourier transform of the disturbance field have been used to construct the solution to the three components of the disturbance velocity in the outer region.

The velocity decays like R^{-1} in the viscous region and is close to the Stokeslet field. In the far inviscid region, the decaying laws are found for the three velocity components in the three directions. The normal velocity is cylindrically symmetric, $U_z = U_z(X, \rho)$, at distances large compared with the Saffman length L_S. It decays like $R^{-5/3}$ in the median plane, $X = 0$. The transversal velocity U_y decays even slower, like $R^{-4/3}$ along the Y axis. The longitudinal component U_x is smaller than the other velocity components within the inviscid region. However, it is the largest one within viscous wakes. The widths of the two wakes that arise around a sphere in a linear shear are $Z_w^{sh} \sim Y_w^{sh} \sim |X|^{1/3}$. The maximum longitudinal and normal velocities in the cores of the wakes decay like $|X|^{-2/3}$ and $|X|^{-1}$, respectively.

Pair-wise particle interactions in the far region of a shear flow are then considered. Even though the problem is essentially unsteady, it can be reduced to the calculation of a quasi-steady disturbance field induced by an isolated particle. When two particles

interact through their outer regions, the migration velocity of each particle is the sum of the migration velocity due to the effect of the particle itself and the disturbance velocity induced by the other particle. The particles repel when they are placed in the transversal directions. The particles approach when their line of centres is nearly parallel to the slip velocity.

E.S.A. gratefully acknowledges the hospitality of ESPCI during the preparation of this work.

REFERENCES

Abramowitz, M. & Stegun, I. 1964 *Handbook of Mathematical Functions with Formulas, Graphs and Mathematical Tables*. US Government Printing Office: Nat. Bur. Standards.

Asmolov, E. S. 1990 Dynamics of a spherical particle in a laminar boundary layer. *Fluid Dyn.* **25**, 886–890.

Asmolov, E. S. 1999 The inertial lift on a spherical particle in a plane Poiseuille flow at large channel Reynolds number. *J. Fluid Mech.* **381**, 63–87.

Conte, S. D. 1966 The numerical solution of linear boundary value problems. *SIAM Rev.* **8**, 309.

Elrick, D. E. 1962 Source functions for diffusion in uniform shear flow. *Austral. J. Phys.* **15**, 283.

Feuillebois, F. 2004 *Perturbation Problems at Low Reynolds Number*. Lecture Notes of Center of Excellence of Advanced Materials and Structures, vol. 15. Polish Academy of Sciences.

Godunov, S. K. 1961 Numerical solution of boundary-value problems for systems of linear ordinary differential equations. *Usp. Mat. Nauk* **16** (3), 171–174 (in Russian).

Harper, E. Y. & Chang, I.-D. 1968 Maximum dissipation resulting from lift in a slow viscous shear flow. *J. Fluid Mech.* **33**, 209–225.

Kaneda, Y. & Ishii, K. 1982 The hydrodynamic interaction of two spheres moving in an unbounded fluid at small but finite Reynolds number. *J. Fluid Mech.* **124**, 209–217.

Kulkarni, P. M. & Morris, J. F. 2008 Pair-sphere trajectories in finite-Reynolds-number shear flow. *J. Fluid Mech.* **596**, 413–435.

Lin, C. J., Peery, J. H. & Schowalter, W. R. 1970 Simple shear flow round a rigid sphere: inertial effects and suspension rheology. *J. Fluid Mech.* **44**, 1–17.

Matas, J.-P., Glezer, V., Guazzelli, E. & Morris, J. F. 2004 Trains of particles in finite-Reynolds-number pipe flow. *Phys. Fluids* **11**, 4192–4195.

McLaughlin, J. B. 1991 Inertial migration of a small sphere in linear shear flows. *J. Fluid Mech.* **224**, 261–274.

McLaughlin, J. B. 1993 The lift on a small sphere in wall-bounded linear shear flows. *J. Fluid Mech.* **246**, 249–265.

Mikulencak, D. R. & Morris, J. F. 2004 Stationary shear flow around fixed and free bodies at finite Reynolds number. *J. Fluid Mech.* **520**, 215–242.

Miyazaki, K., Bedeaux, D. & Avalos, J. B. 1995 Drag on a sphere in slow shear flow. *J. Fluid Mech.* **296**, 373–390.

Poe, G. G. & Acrivos, A. 1975 Closed-streamline flows past rotating single cylinders and spheres: inertia effects. *J. Fluid Mech.* **72**, 605–623.

Proudman, I. & Pearson, J. R. A. 1957 Expansions at small Reynolds numbers for the flow past a sphere and a circular cylinder. *J. Fluid Mech.* **2**, 237–262.

Saffman, P. G. 1965 The lift on a small sphere in a slow shear flow. *J. Fluid Mech.* **22**, 385–400.

Saffman, P. G. 1968 Corrigendum. *J. Fluid Mech.* **31**, 624.

Schonberg, J. A. & Hinch, E. J. 1989 Inertial migration of a sphere in Poiseuille flow. *J. Fluid Mech.* **203**, 517–524.

Sidorov, Y. V., Fedoryuk, M. V. & Shabunin, M. I. 1976 *Lectures on the Theory of the Functions of Complex Variable*. In Russian. Nauka.

Subramanian, G. & Koch, D. L. 2006 Inertial effects on the transfer of heat or mass from neutrally buoyant spheres in a steady linear velocity field. *Phys. Fluids* **18**, 073302.

Vasseur, P. & Cox, R. G. 1977 The lateral migration of spherical particles sedimenting in a stagnant bounded fluid. *J. Fluid Mech.* **80**, 561–591.